Journal of the Korean Nuclear Society
Volume 28, Number 5, pp. 488~499, October 1996

Extension of Source Projection Analytic Nodal S_N Method for Analysis of Hexagonal Assembly Cores

Tae Hyeong Kim and Nam Zin Cho
Korea Advanced Institute of Science and Technology
Department of Nuclear Engineering
373-1 Kusong-dong, Yusong-gu, Taejon, Korea 305-701

(Received April 4, 1996)

Abstract

We have extended the source projection analytic nodal discrete ordinates method (SPANDOM) for more flexible applicability in analysis of hexagonal assembly cores. The method (SPANDOM-FH) does not invoke transverse integration but instead solves the discrete ordinates equation analytically after the source term is projected and represented in hybrid form of high-order polynomials and exponential functions. SPANDOM-FH which treats a hexagonal node as one node is applied to two fast reactor benchmark problems and compared with TWOHEX.

The results of comparison indicate that the present method SPANDOM-FH predicts accurately k_{eff} and flux distributions in hexagonal assembly cores. In addition, SPANDOM-FH gives the continous two-dimensional intranodal scalar flux distributions in a hexagonal node. The reentering models between TWOHEX and SPANDOM were also compared and it was confirmed that SPANDOM's model is more realistic.

Through the results of benchmark problems, we conclude that SPANDOM-FH has the sufficient accuracy for the nuclear design of fast breeder reactor (FBR) cores with hexagonal assemblies.

1. Introduction

The transport equation used in nuclear reactor and radiation shielding application is a linear Boltzmann equation which was first formulated for the study of the kinetic theory of gases. Several numerical schemes developed in the past few decades have been successfully implemented for the solution of the neutron transport equation[1~3].

Nodal transport methods are computationally more efficient than conventional finite-difference method and, in general, yield more accurate solutions. The conventional finite-difference schemes require a fine spatial mesh, usually of the order of a mean free path to yield an acceptable accuracy. Therefore, a great deal of effort has been devoted to developing and improving these nodal methods in solving the multi-dimensional transport equation[4, 5].

The discrete ordinates (S_N) method is one of the main means for obtaining numerical solutions to the integro-differential form of the transport equation. It consists of evaluating the transport equation in discrete angular directions. The S_N methods have been widely applied to Cartesian geometry but applications to other geometries are relatively limited.

Hexagonal assemblies have been used in fast

breeder reactors (FBRs) and high conversion light water reactors (HCLWRs) in order to enhance the conversion ratio by hardening the neutron spectrum by means of the reduction of moderator to fuel volume ratio. Recently, hexagonal assemblies are also employed for boron neutron capture therapy (BNCT) reactor to obtain high intensity of epithermal neutrons.

There are various S_N schemes which can treat hexagonal assembly as one node or by dividing a hexagon into triangles. The diamond difference formula and the finite element technique have been applied to the discrete ordinates method for triangular geometry[2, 3]. Flat source approximation is used in diamond difference-like schemes and weighted residual formulation is used to derive a set of equations relating the spatial fluxes in the finite element schemes. Walters combined the linear-nodal method with the linear-characteristic method in rectangular geometry to solve the transport equation on an equilateral triangular node[6]. Paternoster and Walters extended the linear-characteristic-nodal scheme to a general triangular node[7].

The use of the flat source approximation or the low-order spatial expansion of the node interior source and of the surface angular flux possesses some limitations, that is, it limits the node sizes, especially, in regions where the flux varies rapidly.

In recent years the transverse integration procedure has been used when deriving the nodal coupling equations in hexagonal geometry calculation[8~10]. This procedure integrates the multidimensional transport equation over three transverse spatial directions to reduce it to a differential equation in each spatial direction. Each equation is then solved and the resulting integrals are evaluated by assuming the spatial distribution of flux, source, and transverse leakage. The transverse integration used causes difficulties in the treatment of the transverse leakage shape as in the diffusion nodal methods in hexagonal geometry. For a hexagonal node, since the boundary line on which the transverse leakage is defined contains vertex points, the transverse leakage is no longer continuous at node center. To treat this discontinuity Mauger[8] divided a hexagonal node into two half-hexagons for a spatial sweep and Wagner[9] imbedded the discontinuity into the elements of response matrices using the block inversion technique. Ikeda and Takeda[10] used the "divided flat approximation" considering the discontinuity at node center. These nodal methods with transverse integration procedure give not the intranodal flux distribution but the integral nodal quantities only, although the calculational accuracy is high and the computing time is reduced.

In this paper, the new nodal S_N method called the source projection analytic nodal discrete ordinates method (SPANDOM)[11, 12] is extended to the "one node per hexagon" calculation for its more flexible application in analysis of hexagonal assembly cores. The SPANDOM method was successfully applied to the triangular geometry and half-hexagonal geometry[12].

The features of SPANDOM are (1) it does not invoke transverse integration but instead directly solves the two-dimensional S_N equation, (2) the scalar flux and source distribution are projected and represented in high-order polynomials and/or exponential functions, and (3) the solution of the S_N equation is decomposed into its particular and homogeneous parts. The particular solution is then analytically solved from the source distribution. The homogeneous solution is expanded in terms of the analytic basis solutions of the homogeneous transport equation and the boundary conditions.

The paper is organized as follows. Section 2 presents a brief review on SPANDOM. In Section 3, we provide its extension for full-hexagonal node calculation. Section 4 presents numerical results for two fast reactor benchmark problems and a non-reentering problem. Finally, conclusions of the study shall be given in Section 5.

2. Overview of SPANDOM

As our starting point for the SPANDOM, we take the following two-dimensional discrete ordinates transport equation for angular direction n and energy group g:

$$M\psi_{ng}(x,y)=\mu_n\frac{\partial\psi_{ng}}{\partial x}+\eta_n\frac{\partial\psi_{ng}}{\partial y}+\sigma_g\psi_{ng}=S_g(x,y), \quad (1)$$

where

μ_n, η_n = x-, y-direction cosines of the particle direction,

σ_g = macroscopic total cross section,

$S_g(x, y)$ = source term which contains the scattering and fission emission.

In the above equation, we assume that the source term, $S_g(x, y)$, is isotropic. In the equilateral triangular or hexagonal geometry, we consider the angular quadrature sets with sixfold symmetry. Hereafter the angular direction and energy group subscripts are omitted for simplicity.

In SPANDOM, we first express the solution of Eq. (1), $\psi(x, y)$, as composed of a particular and a homogeneous solution and decompose Eq. (1) into its particular and homogeneous parts:

$$M\psi^p(x,y)=S(x,y), \quad (2)$$

$$M\psi^h(x,y)=0. \quad (3)$$

Now we assume in Eq. (2) that the source distribution in the node is represented by a polynomial function and/or exponential function. The particular solution of Eq. (1) can then be easily expressed in the following form:

$$\psi^p(x,y)=M^{-1}S(x,y). \quad (4)$$

On the other hand, the homogeneous solution of Eq. (1), $\psi^h(x, y)$, is obtained with the basis solutions of the homogeneous equation, Eq. (3), and the boundary conditions at the node boundary. If a finite number of meaningful boundary conditions are given along the node boundary, the homogeneous solution can be expressed by a finite sum of the basis solutions of Eq. (3). Thus, in a given node we choose N discrete boundary conditions (i.e., integral values or point values) and approximate the homogeneous solution with a linear combination of N basis solutions of the homogeneous equation in the following form:

$$\psi^h(x,y)=\sum_{l=1}^{L}e^{-\sigma'\alpha_l(x,y)}\sum_{k=1}^{K_l}C_{lk}f_k(\xi), \quad (5)$$

where

$$\alpha_l(x,y)=(\beta_l\eta'+1)x-\beta_l y,\quad \sigma'=\frac{\sigma}{\mu},$$

$$\eta'=\frac{\eta}{\mu},\quad \xi=y-\eta' x, \quad (6)$$

and $N=\sum_{l=1}^{L}K_l$. In Eq. (5), if $f(\xi)$ and β are given, the expansion coefficients c_{lk} can be determined using N boundary conditions. The boundary condition (B. C.) for the homogeneous solution is expressed by

$$\text{B.C.}^{\psi_h}=\text{B.C.}^{\psi}-\text{Boundary Value}^{\psi_p}. \quad (7)$$

3. SPANDOM for Hexagonal Geometry Calculations

The applications of SPANDOM to triangular geometry and half-hexagonal geometry were reported elsewhere[11, 12] and its application to full-hexagonal geometry is straightforward. The scalar fluxes (vertex fluxes, surface-averaged fluxes, node-averaged flux, etc.) obtained by the conventional S_N quadrature formula are used for the construction of the source distribution in within-group scattering iterations and fission source iterations.

Given a nodal geometry, the particular solution of Eq. (1) can be easily obtained by Eq. (4) after the source distribution in the node is represented by appropriate shape function such as polynomial function and/or exponential function, as we shall see later.

In the homogeneous solution expansion, the arbitrary function $f(\xi)$ and arbitrary constant β are appropriately chosen for the simplicity of derivation and boundary condition representation. The vertex angular fluxes and the surface-averaged angular fluxes are

taken as the boundary conditions.

3.1. Triangle Approach (SPANDOM-TA) and Half Hexagon Approach(SPANDOM-HH)

In triangle approach and half-hexagon approach, a hexagonal node is partitioned into six equilateral triangular nodes as shown in Fig. 1. In each triangular node we project and approximate the source distribution in a third-order polynomial function about the centroid of the triangle:

$$S(x, y) = s_1 + s_2X + s_3Y + s_4X^2 + s_5XY + s_6Y^2 + s_7(X^3 - 3XY^2), \quad (8)$$

where $X=x-x_c$, $Y=y-y_c$, and (x_c, y_c) are the coordinates of the centroid. The coefficients s_1, s_2, ···, s_7 are expressed in terms of the three vertex sources, three surface-averaged sources, and one node-averaged source as shown in Fig. 1. The particular solution is then easily obtained using a similar third-order polynomial function as in Eq. (4).

In half-hexagon approach, unlike the triangle approach which treats six triangles independently, we consider two half-hexagons each of which consists of three triangular subnodes and can obtain continuous angular flux distribution in a half-hexagon, although source distribution is defined in each subnode.

Both approaches are solved by considering two different neutron incoming cases. The detail description of these approaches is given in Ref. [12].

3.2. Full-Hexagon Approach (SPANDOM-FH)

In full-hexagon approach, a hexagonal assembly is considered as one node. From many experiences not shown here, we note that it is necessary to reflect more actual intra-node source distribution in order to achieve acceptable accuracy in one-node per hexagon calculation. To do this, we consider the following directional source "skewness" using the coordinate system of hexagonal node in Fig. 2:

$$\Delta S_x = \int_0^{h/2} dx \int_{-\frac{x}{\sqrt{3}}}^{\frac{x}{\sqrt{3}}} S(x, y)dy - \int_{-h/2}^{0} dx \int_{\frac{x}{\sqrt{3}}}^{-\frac{x}{\sqrt{3}}} S(x, y)dy, \quad (9a)$$

$$\Delta S_u = \int_{-h/2}^{0} dx \int_{-\frac{x}{\sqrt{3}}-\frac{h}{\sqrt{3}}}^{\frac{x}{\sqrt{3}}} S(x, y)dy - \int_0^{h/2} dx \int_{\frac{x}{\sqrt{3}}}^{-\frac{x}{\sqrt{3}}+\frac{h}{\sqrt{3}}} S(x, y)dy, \quad (9b)$$

$$\Delta S_p = \int_{-h/2}^{0} dx \int_{-\frac{x}{\sqrt{3}}}^{\frac{x}{\sqrt{3}}+\frac{h}{\sqrt{3}}} S(x, y)dy - \int_0^{h/2} dx \int_{\frac{x}{\sqrt{3}}-\frac{h}{\sqrt{3}}}^{-\frac{x}{\sqrt{3}}} S(x, y)dy. \quad (9c)$$

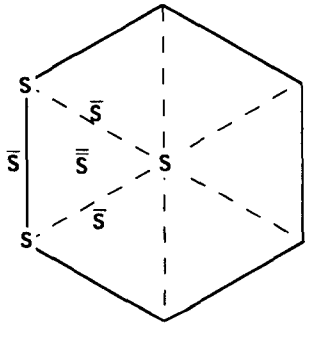

Fig. 1. Source terms used in SPANDOM-TA and SPANDOM-HH

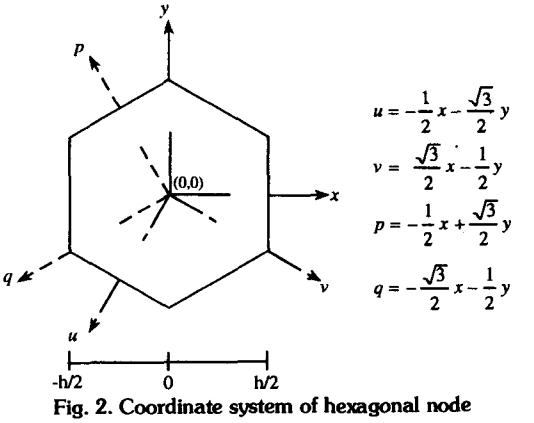

Fig. 2. Coordinate system of hexagonal node

In the hexagonal node we project and approximate the source distribution with hybrid form of third-order polynomial function and exponential function:

$$S(x,y) = s_1 + s_2x + s_3y + s_4x^2 + s_5xy + s_6y^2 + s_7(x^3 - 3xy^2) + s_8(e^{\kappa x} - e^{-\kappa x}) + s_9(e^{\kappa u} - e^{-\kappa u}) + s_{10}(e^{\kappa p} - e^{-\kappa p}) \quad (10)$$

The coefficients s_1, s_2, $\cdots$, s_{10} in Eq. (10) are expressed in terms of the one node-averaged source, six surface-averaged sources, and three directional source skewnesses. The particular solution is then easily obtained by Eq. (4), that is,

$$\psi^p(x,y) = c_1 + c_2x + c_3y + c_4x^2 + c_5xy + c_6y^2 + c_7(x^3 - 3xy^2) + c_8e^{\kappa x} + c_9e^{-\kappa x} + c_{10}e^{\kappa u} + c_{11}e^{-\kappa u} + c_{12}e^{\kappa p} + c_{13}e^{-\kappa p} . \quad (11)$$

In the above Eqs. (10) and (11), the exponent coefficient k should be less than total cross section σ since if $k>\sigma$, one coefficient among $c_8 \sim c_{13}$ may be infinite. To determine the exponent coefficient we consider eigenvalues of the one-dimensional homogeneous transport equation,

$$\mu \frac{\partial \psi}{\partial x}(x,\mu) + \psi(x,\mu) = \frac{c}{2}\int_{-1}^{1}\psi(x,\mu')d\mu' , \quad (12)$$

where c is the scattering ratio. The solutions of Eq. (12) can be obtained with the eigenfunctions which have the corresponding eigenvalues, ν. The eigenvalues are solutions of the equation[13]

$$\Lambda(\nu) \equiv 1 - \frac{c\nu}{2}\int_{-1}^{1}\frac{d\mu}{\nu - \mu} = 1 - c\nu \tanh^{-1}\left(\frac{1}{\nu}\right) = 0 . \quad (13)$$

There are only two zeros of $\Lambda(\nu)$, and for $c<1$, $\Lambda(\nu)$, has one zero on the positive real axis between $+1$ and $+\infty$ and a corresponding zero on the negative real axis. It is easily seen that as c approaches 0, the root ν_0 of $\Lambda(\nu)$ approaches unity and as c approaches 1, ν_0 approaches ∞. As c varies between 0 and 1, ν_0 varies monotonically between 1 and ∞. Therefore, we take the exponent coefficient, k, as the root of Eq. (14),

$$\tanh^{-1}\left(\frac{x}{\sigma}\right) = \frac{x}{c\sigma} . \quad (14)$$

For the homogeneous solution expansion, four vertex angular fluxes (ψ_1, ψ_2, ψ_3, ψ_4) and three surface-averaged angular fluxes ($\bar{\psi}_T$, $\bar{\psi}_C$, $\bar{\psi}_B$) are taken as the boundary conditions as shown in Fig. 3. The following homogeneous solution is used for calculation:

$$\psi^h(x,y) = \begin{cases} [T_1 + T_2\xi + T_3\xi^2]e^{-\sigma'\{(\beta_T\eta'+1)x - \beta_T y\}} \\ \quad \text{for } \eta'x + \dfrac{1+\sqrt{3}\eta'}{2\sqrt{3}}h \le y \le y_s(x) \\ [C_1 + C_2\xi + C_3\xi^2]e^{-\sigma'\{(\beta_C\eta'+1)x - \beta_C y\}} \\ \quad \text{for } \eta'x - \dfrac{1-\sqrt{3}\eta'}{2\sqrt{3}}h \le y \le \eta'x + \dfrac{1+\sqrt{3}\eta'}{2\sqrt{3}}h \\ [B_1 + B_2\xi + B_3\xi^2]e^{-\sigma'\{(\beta_B\eta'+1)x - \beta_B y\}} \\ \quad \text{for } -y_s(x) \le y \le \eta'x - \dfrac{1-\sqrt{3}\eta'}{2\sqrt{3}}h \end{cases} \quad (15)$$

where

$$-\frac{h}{2} \le x \le \frac{h}{2} , \quad y_s(x; x<0) = \frac{x}{\sqrt{3}} + \frac{h}{\sqrt{3}} ,$$

$$y_s(x; x>0) = \frac{-x}{\sqrt{3}} + \frac{h}{\sqrt{3}} , \quad \beta_T = \frac{\sqrt{3}}{1-\sqrt{3}\eta'} ,$$

$$\beta_C = 0, \quad \beta_B = \frac{-\sqrt{3}}{1+\sqrt{3}\eta'} . \quad (16)$$

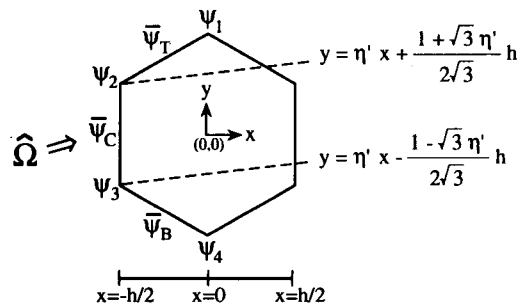

Fig. 3. Boundary conditions for homogeneous solution

The constants β's in Eq. (15) are chosen such that the exponential functions in each equation vanish at neutron incoming boundaries. The boundary conditions are used to determine the coefficients T_i, C_i, and B_i for $i=1, 2, 3$.

4. Numerical Results

The accuracy of SPANDOM-FH has been tested on two fast reactor benchmark problems. The first problem is the KNK-II benchmark problem of the NEACRP benchmark problems[14] and the second is a modified SNR-300 benchmark problem[15]. The numerical results are compared with those of TWOHEX[16] obtained using a spatial mesh of six triangles per hexagon (it will be referred to as TWOHEX-6△). TWOHEX uses the discrete ordinates approximation for the angular variation of particle distribution and a linear-characteristic-nodal scheme for spatial discretization. In addition to TWOHEX-6△, the results of SPANDOM-TA are also given.

The reference solutions for all problems were obtained with TWOHEX using a spatial mesh of 96 triangles per hexagon (TWOHEX-96△). SPANDOM and TWOHEX use the same angular quadrature sets. The convergence criterion of 5×10^{-6} was used for the eigenvalue calculation.

4.1. 2-D KNK-II Benchmark Problem

The KNK-II problem is a four-group, eight-ring representation of a fast breeder reactor with a small central test zone. The transport effect is accentuated due to small size of the core and the local insertion of control rods.

Table 1 shows the results of region-averaged group fluxes and k_{eff} comparisons of TWOHEX-6△ and SPANDOM. SPANDOM-FH agrees with the reference, with difference being less than 0.199%△k. On the other hand, TWOHEX-6△ underestimates k_{eff} by 0.482%△k in the 'rods-in' case. In the 'rods-out' case, TWOHEX-6△ and SPANDOM underestimate k_{eff} by less than 0.1%△k relative to the reference.

It is also seen in Table 1 that the region-averaged flux errors of SPANDOM-TA approach are relatively smaller than those of TWOHEX-6△ and those of SPANDOM-FH approach are comparable to the corresponding TWOHEX-6△ results for both 'rods-in' and 'rods-out' cases.

Note that SPANDOM-TA and SPANDOM-FH "overpredict" the region-averaged fluxes by a few percent in sodium/steel zone. It is suspected that this is caused by the difference in the reentering models in SPANDOM and TWOHEX used in the outermost hexagons next to the vacuum region.

4.2. Modified SNR-300 Benchmark Problem

The original SNR-300 problem is a four-group, two-dimensional fast reactor problem as specified in the ANL benchmark problem book, Problem Identification No. 18-A5[15]. In this study we modified the original SNR-300 problem by adding several radial blankets in the outer region of the core to construct

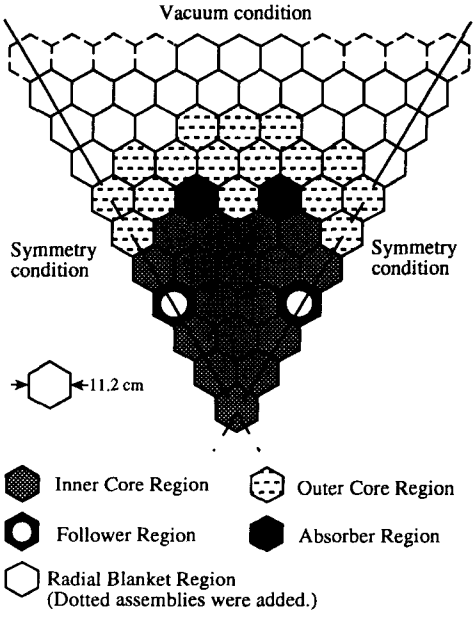

Fig. 4. Modified SNR-300 benchmark problem

Table 1. 2-D KNK-II Benchmark Problem: Percentage Errors of the Region-Averaged Group Fluxes

Region	Rods-in				Rods-out			
	Reference (TWOHEX-96△)	TWOHEX-6△	SPANDOM TA	SPANDOM FH	Reference (TWOHEX-96△)	TWOHEX-6△	SPANDOM TA	SPANDOM FH
Group 1								
Test zone	1.42573E+03*	0.48	−0.14	−0.26	1.14429E+03	0.11	0.07	0.05
Driver without moderator	9.63133E+02	0.09	−0.10	−0.13	8.52569E+02	−0.02	0.00	0.00
Driver with moderator	6.58833E+02	0.22	−0.01	−0.05	5.59082E+02	−0.06	0.11	0.09
Control rod	8.55283E+02	1.01	−0.24	−0.55	–	–	–	–
Control rod follower	–	–	–	–	8.49511E+02	0.28	0.02	−0.08
Reflector without moderator	2.69848E+02	0.94	−0.06	−0.31	2.20368E+02	0.37	0.08	−0.05
Reflector with moderator	2.46828E+02	0.91	−0.07	−0.29	2.04173E+02	0.38	0.07	−0.05
KNK-1 reflector	2.44062E+01	0.36	−0.21	0.18	1.99214E+01	−0.15	−0.05	0.39
Sodium/steel zone	8.33001E+00	0.20	1.03	1.15	6.79551E+00	−0.30	1.19	1.36
Group 2								
Test zone	1.04619E+03	0.24	−0.06	−0.16	9.86685E+02	0.08	0.09	0.09
Driver without moderator	6.99064E+02	−0.17	0.00	0.07	7.28325E+02	−0.20	0.10	0.15
Driver with moderator	4.67159E+02	0.25	−0.05	−0.11	4.48573E+02	0.10	0.07	−0.01
Control rod	6.26531E+02	1.14	−0.22	−0.52	–	–	–	–
Control rod follower	–	–	–	–	7.85343E+02	0.10	0.14	0.09
Reflector without moderator	2.60761E+02	−0.04	0.16	0.18	2.27861E+02	−0.54	0.25	0.43
Reflector with moderator	2.35832E+02	0.01	0.14	0.18	2.08837E+02	−0.47	0.22	0.39
KNK-1 reflector	2.96901E+01	−0.49	−0.18	0.97	2.47506E+01	−1.02	−0.07	1.19
Sodium/steel zone	1.32406E+01	−0.41	1.57	2.07	1.10056E+01	−0.93	1.68	2.29
Group 3								
Test zone	1.80784E+02	−0.78	−0.05	0.18	2.76611E+02	0.03	−0.10	−0.07
Driver without moderator	1.84818E+02	−0.47	−0.34	−0.37	2.68998E+02	0.52	−0.25	−0.46
Driver with moderator	2.44638E+02	−0.13	0.17	0.25	2.56081E+02	−0.07	0.12	0.12
Control rod	1.13881E+02	1.98	−1.11	−1.44	–	–	–	–
Control rod follower	–	–	–	–	3.08168E+02	−0.24	0.00	0.05
Reflector without moderator	1.67395E+02	0.16	0.31	−0.02	1.52041E+02	−0.48	0.33	0.24
Reflector with moderator	1.51568E+02	0.28	0.30	−0.01	1.39549E+02	−0.36	0.31	0.18
KNK-1 reflector	2.27145E+01	−0.26	−0.31	0.66	1.91353E+01	−0.83	−0.26	0.93
Sodium/steel zone	9.67958E+00	−0.50	1.32	2.00	8.13648E+00	−1.06	1.37	2.27
Group 4								
Test zone	5.77105E+00	−4.10	−0.34	6.22	2.91358E+01	−0.80	−0.67	−0.20
Driver without moderator	3.19834E+01	−0.37	−1.11	−1.61	5.67729E+01	2.39	−1.53	−2.06
Driver with moderator	1.21433E+02	−0.51	0.34	0.44	1.30034E+02	−0.44	0.07	0.19
Control rod	6.89855E+00	3.79	−4.73	−4.49	–	–	–	–
Control rod follower	–	–	–	–	8.78099E+01	−2.68	0.03	0.90
Reflector without moderator	1.81595E+02	0.84	−0.24	−0.92	1.64438E+02	0.23	−0.18	−0.68
Reflector with moderator	1.72478E+02	0.98	−0.11	−0.72	1.57062E+02	0.36	−0.07	−0.55
KNK-1 reflector	5.89323E+01	3.51	0.63	−0.83	5.04511E+01	2.96	0.72	−0.63
Sodium/steel zone	1.30513E+01	2.59	0.87	0.71	1.11379E+01	2.05	0.96	0.92
k_{eff}	1.00941	1.00454	1.01055	1.01142	1.30945	1.30833	1.30877	1.30887
ε_{k}(%)	–	−0.482	0.113	0.199	–	−0.096	−0.052	−0.044

S_4 solutions

Normalization: $\sum_g \int_v \nu\sigma_{fg}\,\phi_g\,dV = 10^3$

* Read as 1.42573×10^3

a complete hexagonal geometry as shown in Fig. 4.

Table 2 shows the percentage errors of the region-averaged group fluxes and effective multiplication factors for the 'rods-in' and 'rods-out' cases. SPANDOM-FH accurately predicts k_{eff} with relative differences being less than 0.02%△k, while TWOHEX-6△ underestimates by about 0.1%△k in the 'rods-in' case. In the 'rods-out' case, SPANDOM-FH more accurately estimates k_{eff} by less than ±0.01%△k. In Fig. 5, the percentage errors of the hexagonal node-averaged group fluxes, relative to the TWOHEX-96△ reference solutions, are given for the 'rods-in'. It is seen that the errors of SPANDOM-FH are smaller than those of TWOHEX-6△ in most regions except in the outer blanket assemblies that are located near the vacuum region. This discrepancy in the blanket region is again attributed to the difference in the reentering models. This trend is similar to that of the 2-D KNK-II benchmark problem illustrated in Section 4.1.

Table 2. Modified SNR-300 Benchmark Problem : Percentage Errors of the Region-Averaged Group Fluxes

Region	Rods-in				Rods-out			
	Reference (TWOHEX-96△)	TWOHEX-6△	SPANDOM TA	SPANDOM FH	Reference (TWOHEX-96△)	TWOHEX-6△	SPANDOM TA	SPANDOM FH
Group 1								
Inner core	1.54762E+02*	0.24	−0.05	−0.06	1.32031E+02	0.13	−0.03	0.01
Outer core	8.81647E+01	−0.40	0.06	0.06	9.13561E+01	−0.31	0.04	0.03
Radial blanket	1.34155E+01	−0.16	0.02	−0.02	1.37894E+01	−0.10	0.00	−0.03
Absorber	8.94035E+01	0.56	0.02	−0.17	–	–	–	–
Follower	1.46206E+02	0.52	−0.07	−0.14	1.07737E+02	0.33	0.01	−0.07
Group 2								
Inner core	7.81163E+02	0.19	−0.05	−0.05	7.13379E+02	0.09	−0.03	0.00
Outer core	3.94941E+02	−0.18	0.05	0.05	4.43511E+02	−0.09	0.04	0.01
Radial blanket	1.18211E+02	−0.09	0.23	0.08	1.29585E+02	−0.01	0.22	0.06
Absorber	4.37949E+02	0.42	−0.03	−0.16	–	–	–	–
Follower	8.31478E+02	0.25	−0.05	−0.07	6.12966E+02	0.06	0.00	0.01
Group 3								
Inner core	7.05501E+01	0.14	−0.02	−0.02	6.71215E+01	0.10	−0.04	−0.01
Outer core	3.30299E+01	−0.20	0.00	0.05	4.09106E+01	0.10	−0.05	−0.11
Radial blanket	1.74200E+01	0.00	0.51	0.29	1.93035E+01	0.06	0.47	0.27
Absorber	2.96295E+01	0.91	−0.29	−0.57	–	–	–	–
Follower	8.87135E+01	−0.20	0.19	0.31	6.47433E+01	−0.49	0.22	0.44
Group 4								
Inner core	1.23790E+01	0.02	0.06	0.07	1.24007E+01	0.03	−0.01	0.03
Outer core	4.98320E+00	−0.21	0.09	0.20	7.06467E+00	0.30	−0.06	−0.11
Radial blanket	5.42918E+00	0.10	0.77	0.47	6.09113E+00	0.15	0.71	0.45
Absorber	2.58977E+00	1.86	−0.88	−1.29	–	–	–	–
Follower	1.82291E+01	−0.49	0.39	0.58	1.28602E+01	−0.89	0.39	0.76
k_{eff}	1.13890	1.13784	1.13901	1.13913	1.23677	1.23616	1.23679	1.23668
ε_k(%)	–	−0.093	0.009	0.020	–	−0.049	0.002	−0.007

S_4 solutions

Normalization: $\sum_g \int_v \nu\sigma_{fg}\,\phi_g\,dV = 10^3$

* Read as 1.54762×10^2

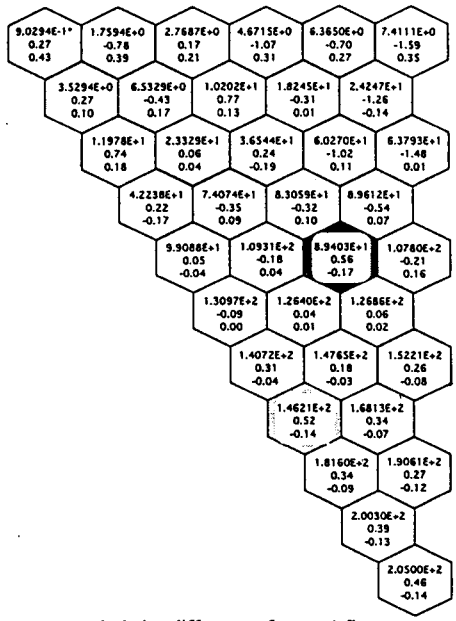

a) Relative difference of group 1 flux

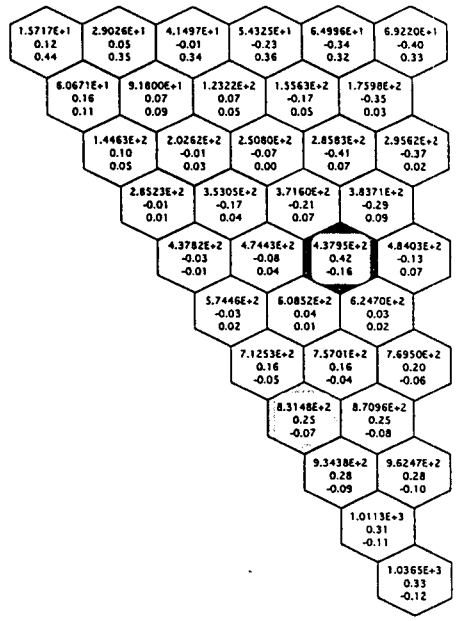

b) Relative difference of group 2 flux

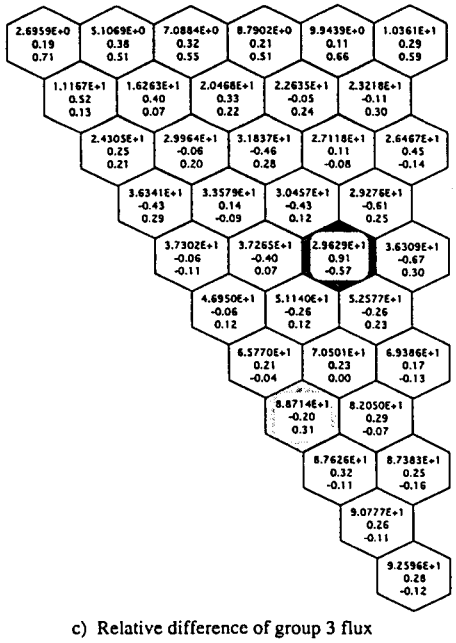

c) Relative difference of group 3 flux

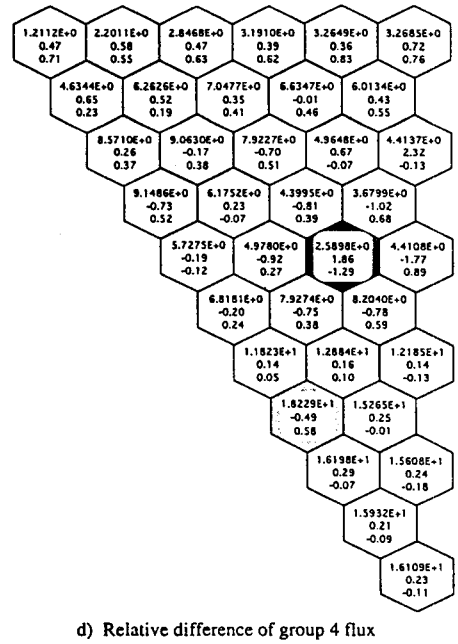

d) Relative difference of group 4 flux

1. * read as 9.0294 x 10^{-1}
2. xx.xx Reference solution (TWOHEX-96Δ)
   x.xx TWOHEX-6Δ error (%)
   x.xx SPANDOM-FH error (%)

Fig. 5. Flux distributions of the modified SNR-300 benchmark problem: 'rods-in' case(1/12 core).

4.3. Non-Reentering Problem Test

Hexagonal geometry with vacuum boundary condition has 'reentrant nodes' in which the escaping particle can reenter the adjacent node. In the outermost hexagon and vacuum interface region, TWOHEX appends imaginary triangular nodes and includes these nodes in the problem domain but SPANDOM models the vacuum region directly as shown in Fig. 6.

To compare the performance of TWOHEX and SPANDOM in the problem without the reentering effect, we made up a simplified hexagonal core as shown in Fig. 7. The regionwise material properties are the same as those of KNK-II problem. However, the core dose not have hexagonal node any more, instead the global shape of the core is hexagonal geometry and has non-reentrant external boundary.

This problem was calculated using TWOHEX with triangle height $h=1.625$cm (for reference) and $h=6.5$cm. and SPANDOM-TA was adopted for comparison since it can treat triangular nodes independently and the reentering models of three SPANDOM approaches are the same. SPANDOM-TA calculation with triangle height $h=6.5cm$ was performed. Table 3 shows the results. We can see that SPANDOM-TA is more accurate than TWOHEX ($h=6.5cm$) at core boundary region (sodium/steel zone) next to the vacuum boundary with non-reentrance.

From the numerical results of the problems with and without reentering effect we conclude that the most discrepancies in the results between SPANDOM and TWOHEX in the boundaries of FBR benchmark problems are caused by the difference of the reentering models between TWOHEX and SPANDOM. Since the reentering model in SPANDOM is physically more realistic than that of TWOHEX, the SPANDOM results should be more accurate.

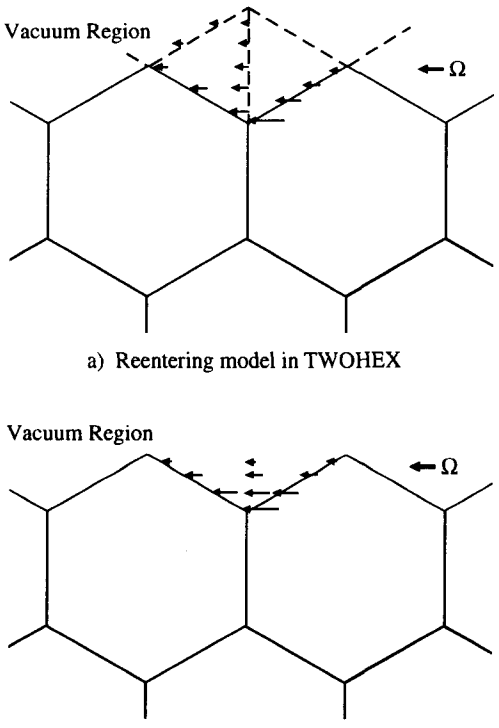

Fig. 6. Reentering models in TWOHEX and SPANDOM

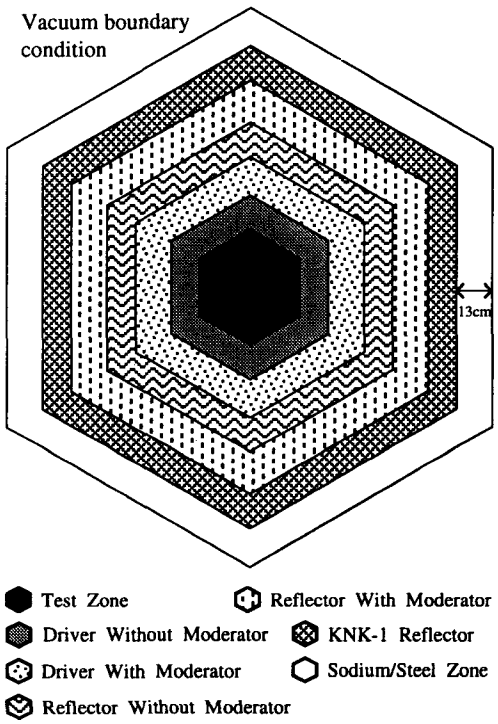

Fig. 7. Simplified hexagonal core problem with non-reentrant boundary.

Table 3. Simplified Hexagonal Core Problem : Percentage Errors of the Region-Integral Group Fluxes (1/6 Core)

Region	Reference (TWOHEX: h=1.625cm)	TWOHEX (h=6.5cm)	SPANDOM-TA (h=6.5cm)
Group 1			
Test zone	7.119779E+03*	0.09	−0.02
Driver without moderator	9.242257E+03	0.03	0.00
Driver with moderator	7.656667E+03	−0.03	0.16
Reflector without moderator	3.601145E+03	0.28	0.13
Reflector with moderator	9.666013E+02	0.26	−0.05
KNK-1 reflector	3.473507E+02	−0.20	−0.24
Sodium/steel zone	1.254093E+02	−0.22	−0.21
Group 2			
Test zone	6.617379E+03	0.09	0.00
Driver without moderator	8.456116E+03	−0.08	0.07
Driver with moderator	6.285657E+03	0.08	0.07
Reflector without moderator	3.966621E+03	−0.41	0.29
Reflector with moderator	1.030637E+03	0.45	0.02
KNK-1 reflector	4.606291E+02	−1.08	−0.46
Sodium/steel zone	2.263123E+02	−0.74	−0.35
Group 3			
Test zone	1.488798E+03	−0.12	−0.16
Driver without moderator	2.427597E+03	0.15	−0.34
Driver with moderator	3.548436E+03	−0.04	0.19
Reflector without moderator	2.681855E+03	−0.53	0.46
Reflector with moderator	9.363668E+02	0.64	0.10
KNK-1 reflector	3.654280E+02	−1.22	−0.72
Sodium/steel zone	1.730710E+02	−1.04	−0.62
Group 4			
Test zone	5.797758E+01	−1.22	−1.32
Driver without moderator	3.000446E+02	1.45	−2.10
Driver with moderator	1.752890E+03	−0.36	0.36
Reflector without moderator	2.793001E+03	0.11	−0.07
Reflector with moderator	2.763265E+03	0.48	0.53
KNK-1 reflector	9.712740E+02	2.99	0.29
Sodium/steel zone	2.288254E+02	2.25	−0.34
k_{eff}	1.49208	1.49132	1.49132
ε_R(%)	−	−0.05	−0.05

S_4 solutions

Normalization: $\sum_g \int_v \nu\sigma_{fg}\,\phi_g\,dV = 6\times10^3$

* Read as 7.119779×10^3

The computational efficiency of the nodal discrete ordinates methods depends crucially upon the efficient acceleration schemes for the within-group scattering source iteration and fission source iteration. In the present version of SPANDOM, the asymptotic source extrapolation (ASE) method is used. The computing times are compared in Table 4. The results in Table 4 indicate that SPANDOM is faster than TWOHEX-6△ by factors of 1.1 to 2.8.

Table 4. Comparison of Computation Times*

		KNK-II Problem		Modified SNR-300 Problem	
		rods-in	rods-out	rods-in	rods-out
TWOHEX-6△**		120	103	282	245
SPANDOM†	TA	56	56	202	158
	FH	43	41	148	115

* All calculations are performed with S_4 quadrature. Second(on SUN 4/75).

** Chebyshev acceleration method is used.

† ASE acceleration method is used.

5. Conclusions

We have extended SPANDOM for its more flexible applicability in analysis of hexagonal assembly cores. The method SPANDOM-FH does not invoke transverse integration procedure but instead solves the discrete ordinates equation analytically after the source term is projected and represented in hybrid form of high-order polynomials and exponential functions. SPANDOM-FH is applied to two fast reactor benchmark problems and compared with TWOHEX. The results of comparison indicate that the present method SPANDOM-FH predicts accurately not only effective multiplication factor but also flux distributions in hexagonal geometry.

In addition, through the calculation of a simplified non-reentering problem the reentering models between TWOHEX and SPANDOM were compared and it was confirmed that SPANDOM's model is more realistic.

It is also worth noting that SPANDOM-FH gives the continuous two-dimensional intranodal scalar flux distributions in a hexagonal node but that the other S_N methods which can treat the hexagonal nodes give only the node-averaged quantities. From the res-

ults of benchmark calculations, we conclude that SPANDOM-FH has the sufficient accuracy for the nuclear design of FBR cores with hexagonal assemblies.

Acknowledgment

This work was supported in part by the Korea Science and Engineering Foundation through the Center for Advanced Reactor Research at the Korea Advanced Institute of Science and Technology (KAIST).

References

1. R. Sanchez and N. J. McCormick, "A Review of Neutron Transport Approximation," *Nucl. Sci. Eng.*, **80**, 481 (1982)
2. J. J. Duderstadt and W. R. Martin, *Transport Theory*, Wiley, NY (1979)
3. E. E. Lewis and W.F. Miller, Jr., *Computational Methods of Neutron Transport*, Wiley, NY (1984)
4. R. D. Lawrence, "Progress in Nodal Methods for the Solution of the Neutron Diffusion and Transport Equations," *Prog. Nucl. Energy*, **17**, 271 (1986)
5. A. Badruzzaman, "Nodal Methods in Transport Theory," *Advances in Nuclear Science and Technology*, Vol. 21, p. 1, Plenum Press, New York (1990)
6. W. F. Walters, "The TLC Scheme for Numerical Solution of the Transport Equation on Equilateral Triangular Meshes," *Proc. of the ANS Topical Mtg. on Advances in Reactor Computations*, Vol. I, p. 151, Salt Lake City, UT (March 1983)
7. R. R. Paternoster and W. F. Walters, "The Nodal Transport Method for General Triangular Meshes in (x, y)-Geometry," *Prog. Nucl. Energy*, **18**, 153 (1986)
8. R. L. Mauger, "A Nodal Transport Theory Method in Hexagonal Geometry," *Prog. Nucl. Energy*, **18**, 145 (1986)
9. M. R. Wagner, "Three-Dimensional Nodal Diffusion and Transport Theory Methods for Hexagonal-z Geometry," *Nucl. Sci. Eng.*, **103**, 377 (1989)
10. H. Ikeda and T. Takeda, "A New Nodal S_N Tran sport Method for Three-Dimensional Hexagonal Geometry," *J. Nucl. Sci. Technol.*, **31[6]**, 497 (1994)
11. T. H. Kim and N. Z. Cho, "SPANDOM-Source Projection Analytic Nodal Discrete Ordinates Method," *Proc. Korean Nuclear Society Autumn Mtg.*, Seoul, Korea, October 29, 1994, p. 111, Korean Nuclear Society (1994)
12. T. H. Kim and N. Z. Cho, "Source Projection Analytic Nodal S_N Method for Hexagonal Geometry," *Ann. Nucl. Energy*, **23**, 133 (1996)
13. K. M. Case and P. F. Zweifel, *Linear Transport Theory*, Addison-Wesley Publishing Company, Inc. (1967)
14. T. Takeda and H. Ikeda, *Three-Dimensional Neutron Transport Benchmarks*, NEACRP-L-330 (1991)
15. *Benchmark Problem Book*, ANL-7416, Suppl. 3, p. 861, Argon National Laboratory (1985)
16. W. F. Walters *et al.*, *User's Guide for TWOHEX: A Code Package for Two-Dimensional, Neutral-Particle, Transport in Equilateral Triangular Meshes*, LA-10258-M, Los Alamos National Laboratory (1989)